2013-12-17

Creating a Single Twin Boundary between Two CdTe (111) Wafers

UTD AUTHOR(S): Ce Sun, Ning Lu, Jinguo Wang, Jihyung Lee Xin, Peng and Moom J. Kim

Creating a single twin boundary between two CdTe (111) wafers with controlled rotation angle by wafer bonding

Ce Sun,[1] Ning Lu,[1] Jinguo Wang,[1] Jihyung Lee,[1] Xin Peng,[1] Robert F. Klie,[2] and Moon J. Kim[1,a)]
[1]*Department of Materials Science and Engineering, The University of Texas at Dallas, Richardson, Texas 75080, USA*
[2]*Department of Physics, University of Illinois at Chicago, Chicago, Illinois 60607, USA*

(Received 4 September 2013; accepted 21 November 2013; published online 17 December 2013)

The single twin boundary with crystallographic orientation relationship $(\bar{1}\bar{1}\bar{1})//(111)$ $[0\bar{1}1]//[01\bar{1}]$ was created by wafer bonding. Electron diffraction patterns and high-resolution transmission electron microscopy images demonstrated the well control of the rotation angle between the bonded pair. At the twin boundary, one unit of wurtzite structure was found between two zinc-blende matrices. High-angle annular dark-field scanning transmission electron microscopy images showed Cd- and Te-terminated for the two bonded portions, respectively. The *I-V* curve across the twin boundary showed increasingly nonlinear behavior, indicating a potential barrier at the bonded twin boundary. © *2013 AIP Publishing LLC*. [http://dx.doi.org/10.1063/1.4844855]

Zinc-blende (ZB) CdTe has drawn great attention as optoelectronics and solar energy conversion materials,[1,2] since its near optimum band gap of 1.6 eV and high absorption coefficient of $>5\times10^5$/cm (Ref. 3). Like other Cd*X* (X = S, Se) compounds, CdTe can be both ZB and wurtzite (WZ) structures, resulting in different electronic properties.[4] The electronic and chemical properties of boundaries with different orientations could be significantly different from the matrix. It has been reported that the twin superlattice with numerous twin boundaries in the III-V[5–8] and II-VI[9–14] semiconductor nanowires along ⟨111⟩ growth orientation of ZB structure can considerably enhance band gap engineering and mechanical behavior in quasi-one-dimensional materials.[15] Lengthwise single twin boundary in bicrystalline nanowires and nanobelts with a growth orientation of [11–2] in cubic system has been rarely reported in Si, III-V, and II-VI semiconductors.[16–22] Measuring the electronic transport properties across the single twin boundary was difficult due to the twin boundary was parallel to the long growth axis and the normal dimension was usually less than 100 nm. As a consequence of the disparity in the band gap and electronic properties of the WZ structure and the ZB structure in III-V and II-VI materials, the one unit of WZ structure at twin boundaries could act as a quantum well or barrier.[7,8] Theoretical models with first-principles pseudopotential method[23–26] and experimental results[27–29] showed that the coexistence of hexagonal WZ structure at the twin boundary of two cubic ZB matrices contributed to the appeared quantum effects. This opened new possibilities for properties and functionalities at the atomic and quantum scales by controlling the twin boundary and modulating the twin densities. Therefore, it is highly demanded and remains a challenge to "create" a single twin boundary in a nanowire or a bulk material in order to understand the electronic and mechanical characteristics of the III-V and II-VI quantum well or barrier.

Wafer bonding, which enables directly integrating two or more single crystal wafers with controlled surfaces and orientation, could act as a key technique to create single boundary.[30–40] Si bicrystals have been successfully fabricated by wafer bonding.[40–42] This technique could open a new route for characterizing and understanding a single quantum well and barrier in II-VI materials. In this study, we show the possibility of creating a single boundary between two identical single crystals. The twin boundary with crystallographic orientation relationship $(\bar{1}\bar{1}\bar{1})//(111)$ $[0\bar{1}1]//[01\bar{1}]$ was created without an amorphous layer at the interface. The interface morphology and atomic arrangement of the bonded boundary were analyzed using high-resolution transmission electron microscopy (HRTEM) and high-angle annular dark-field scanning transmission electron microscopy (HAADF-STEM). The electrical property across the twin boundary was compared with that of the CdTe single crystal.

Commercially available one side polished 5×5 mm^2 p-type CdTe (111) wafers with a thickness of 500 μm were used for the bonding experiments. Out of plane ($2\theta/\omega$ scan) and in-plane (φ scan) X-ray diffraction (XRD) (Ultima III, Rigaku) were used to determine the crystal orientations of the planes and flats, respectively. The root mean square surface roughness (RMS) was measured by atomic force microscopy (AFM) (Dimension 3100, Veeco) in tapping mode. For the cleaning process, samples were rinsed in de-ionized water for 5 s, briefly dipped in hydrochloric acid (15% HCl) for 30 s and then rinsed in de-ionized water for 5 s.[43] The samples were dried under a flow of nitrogen gas, and heated on a hot plate at 110 °C for 5 s to evaporate the de-ionized water absorbed on the surface. After that, the wafer pair was loaded into a vacuum bonder (EV 501, EV Group) immediately, to prevent the oxidation of the CdTe surface. Bonding was performed at 400 °C for 20 h under a pressure of 1 MPa. Local structure was acquired using HRTEM (2100F, JEOL) of Focused Ion Beam (FIB) (Nova 200, FEI) milled cross-sections. The atomic arrangement of the interface was characterized using HAADF-STEM (JEM-ARM200F, JEOL). After wafer bonding, Pt contact pads

a)Author to whom correspondence should be addressed. Electronic mail: moonkim@utdallas.edu

with size of $50 \times 50\ \mu m^2$ were deposited on the cross section of the bonded pair by FIB. The *I-V* characteristics were carried out on a Cascade probe station with a semiconductor characterization system (Keithley 4200, Keithley).

Figure 1 presents typical AFM images over a randomly selected $2 \times 2\ \mu m^2$ area on CdTe (111) surfaces. The RMS changed from 1.84 nm for the as-received wafer to 1.63 nm for the cleaned wafer, which indicated that the surface condition was improved after cleaning. There were some scratches on the surface, as shown in the Figures 1(a) and 1(b). CdTe has a zinc-blende structure with space group $F\bar{4}3m$ at room temperature, and has a three-fold inversion symmetry of the (111) plane. In order to create a twin boundary of two CdTe (111) single crystal wafers, it is required to bond them with a relative rotation angle of 180° (or 60°) around the [111] axis. The flats of the as-received wafers were cut with a random orientation, so in-plane XRD was used to identify their orientations.[44] Wafer bonding was performed by controlling the relative rotation angle of the $[0\bar{1}1]$ directions around the [111] axis.

Figure 2(a) shows the HRTEM image of the bonded pair with a designed relative rotation angle of 180°. As can be seen clearly, the bonded interface was a twin boundary along the $\langle 0\bar{1}1 \rangle$ zone axis. The twin boundary was coherent and atomically sharp. No amorphous layer was found at the interface of the bonded pair, indicated the effectiveness of the cleaning process, and no oxide layer was formed during the bonding process. The diffraction patterns from the left side, at the boundary, and from the right side are presented in the Figures 2(b)–2(d), respectively. Clearly, the diffraction patterns have reconfirmed that the bonded boundary is a $(111)[0\bar{1}1]$ twin boundary. The crystallographic orientation relationship between the two bonded portions is $(\bar{1}\bar{1}\bar{1})//(111)$ and $[0\bar{1}1]//[01\bar{1}]$. A small misorientation angle from the perfect 180° rotation angle may exist due to the lack of precise alignment in the limited bonding chamber. The actual

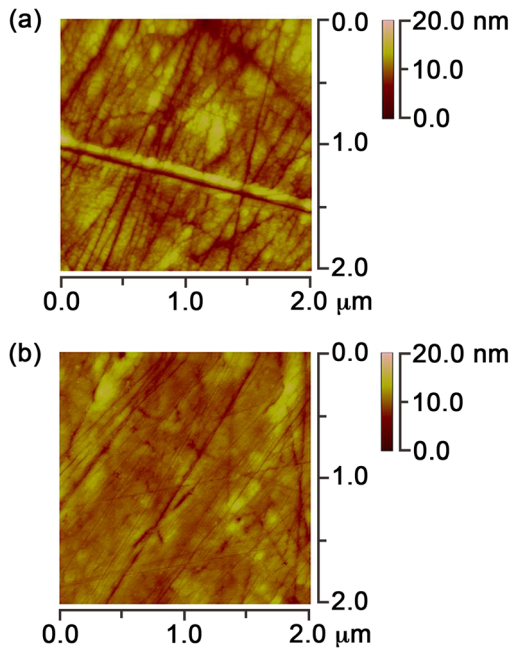

FIG. 1. AFM surface roughness analysis of CdTe surfaces: (a) as-received wafer, and (b) after cleaned wafer.

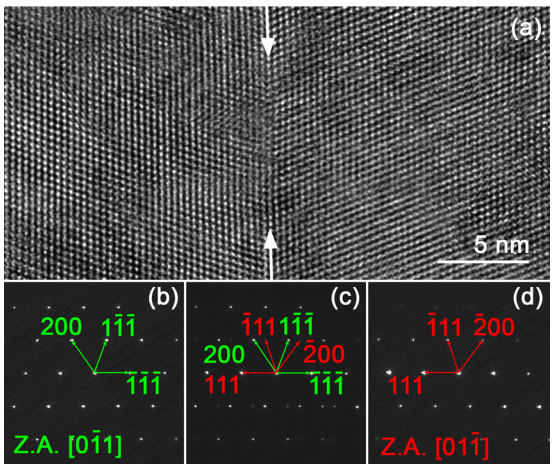

FIG. 2. TEM image (a) of the bonded pair shows the twin boundary with coherent twin interface. The interface is emphasized by the two white arrows. Diffraction patterns for the left (b), interface (c), and right (d) portions of the bonded pair indicated that the crystallographic orientation relationship of the bonded pair was $(\bar{1}\bar{1}\bar{1})//(111)$ and $[0\bar{1}1]//[01\bar{1}]$.

rotation angle was 177.6°, calculated from the recorded tilt angles of both X and Y axes in a double tilt sample holder by aligning the two portions to the $[0\bar{1}1]$ and $[01\bar{1}]$ zone axes, respectively.[45]

Figure 3(a) represents the HAADF-STEM image of the bonded interface, from which the single twin structure was confirmed. It is important to point out that the {111} twin leads to the formation of the CdTe WZ structure at the interface, which was WZ hexagonal instead of ZB cubic. The one unit of CdTe WZ hexagonal structure is highlighted with the green square frame in Figures 3(a) and 3(b). The contrast of the HAADF-STEM image, so-called Z-contrast image, is sensitive to the atomic number of the elements. The atomic

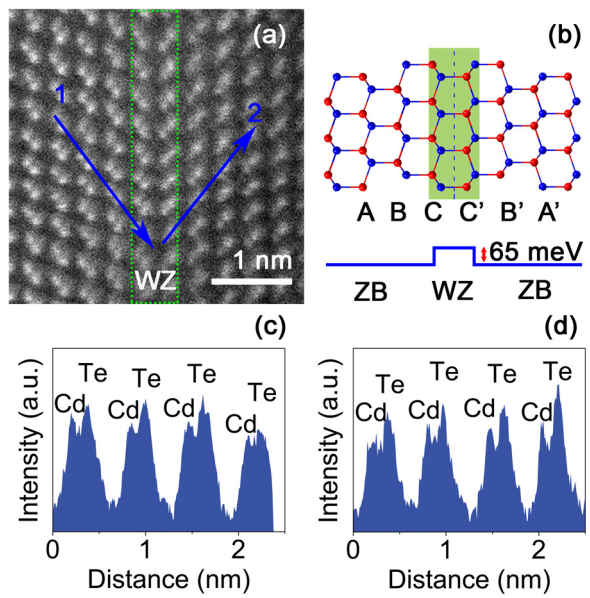

FIG. 3. (a) The $\langle 011 \rangle$ cross-sectional HAADF-STEM image reveals the twin boundary at the bonded interface. (b) The atomic configuration of the bonded twin boundary reveals the two-atomic layer CdTe WZ structure between the CdTe ZB matrices, and conduction band alignment between ZB CdTe and WZ CdTe according to Ref. 24. The red and blue spheres, respectively, represent Cd and Te atoms. HAADF intensity profiles (c) and (d) along the lines 1 and 2 in (a) reveal the atomic arrangement of the bonded interface.

number difference between Cd and Te is large enough for them to appear differently in the image. Te will show brighter dots, when Cd will show with less intensity. Hence, in the high resolution HAADF-STEM image (Figure 3(a)), the dumbbell of Te-Cd was shown along ⟨110⟩, which could be related to specific atomic column in the dumbbell, and to identify the termination of the atoms. HAADF intensity profiles demonstrated that the arrangement of CdTe atoms in the two parts was ordered, Cd- and Te-terminated on the left and right portions, respectively, as shown in Figures 3(c) and 3(d). The low magnification HAADF-STEM image[44] showed well bonded interface in a large area, few voids in the bonded interface were observed which may be caused by surface scratches and rough surfaces. Regarding the tilt/miscut along [110] axis, we did observe one atomic height step along the interface, but rarely, as shown in Fig. S3.[44]

In the present case, the formation of 180° (or 60°) rotational twin alone the ⟨111⟩ axis resulted in a local change in the stacking of the {111}-type close-packed planes, resulting in the formation of a local region of the hexagonal WZ structure, as shown in Figure 3(b). The electronic band structure can differ markedly between WZ and ZB structures in semiconductors, thus the twin interface has a direct impact on the band gap and band structure as hexagonal monolayers. The one unit of WZ structure at twin boundaries could act as quantum well or barrier.[7] The electronic structures of both ZB and WZ CdTe have been calculated using first principles theory.[24] For CdTe, the conduction band (CB) minimum of the WZ structure is 65 meV higher than that of the ZB structure, as shown in Figure 3(b). As a consequence of this, the one unit of CdTe WZ structure at the bonded twin boundary could act as quantum barrier.

Experimentally, twin boundaries in nanowires have been reported frequently, but the results were focused on multiple twin boundaries.[5–15] Lengthwise single twin boundary along the long growth axis in bicrystalline nanowires and nanobelts has been rarely reported.[18–22] It is generally difficult to obtain the electronic transport properties across the single twin boundary due to the limited width of these nanostructures (usually less than 100 nm). In contrast, the single CdTe twin boundary described above, fabricated by wafer bonding, with a width of millimeter level across the twin boundary opens an opportunity to understand the fundamental properties of the a twin boundary WZ quantum barrier, to study the electronic and thermal transport properties. The electrical properties across the twin boundary and of the single crystal are shown in the *I-V* characteristics of Figure 4. The electrical connect configuration was shown in Figure 4 as inset. Pt electrodes, shown in dark yellow and blue, were used for the *I-V* measurement for twin boundary and single crystal, respectively. The slight nonlinear curve of single crystal, red curve as shown in Figure 4, indicated the non-ohmic contact of the Pt/CdTe interface. The *I-V* curve, dark yellow curve as shown in Figure 4, across the twin boundary became increasingly nonlinear with increasing voltage, which indicated that there was a potential barrier at the bonded twin boundary, and coincidence with experimental and theoretical works of III-V and II-VI semiconductors.[46–48]

We have "created" a single twin boundary through wafer bonding technology. Diffraction pattern, HRTEM, and

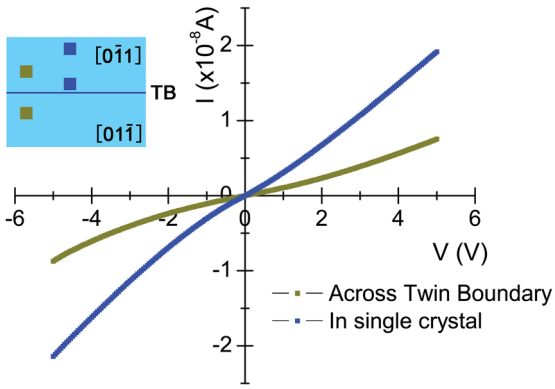

FIG. 4. The *I-V* characteristics were obtained from the CdTe single crystal and across the bonded twin boundary (TB). The inset shows the electrical connection configurations. The Pt electrodes, shown as dark yellow and blue, were used for the *I-V* measurement of the twin boundary and single crystal, respectively.

HAADF-STEM show that the twin boundary was one unit layer of WZ structure between ZB matrices. HAADF-STEM images showed Cd- and Te-terminated for the two bonded portions, respectively. Our preliminary *I-V* characteristics show a potential barrier at the bonded interface, which indicates that the one unit layer of WZ structure between ZB matrices could act as a quantum barrier. The single CeTe twin boundary, fabricated by wafer bonding, opens a new window to understand the fundamental properties of the twin boundary WZ quantum barrier, and to study the electronic and thermal transport properties in the twin boundary and related devices.

This work was supported by DOE BRIDGE (DE-EE0005956).

[1]R. W. Birkmire and E. Eser, Annu. Rev. Mater. Sci. **27**, 625 (1997).
[2]*CdTe and Related Compounds: Physics, Defects, Technology, Hetero- and Nanostructures and Applications: Crystal Growth Technology and Surfaces, Applications*, edited by R. Triboulet and P. Siffert (Elsevier Science & Technology Books, 2009).
[3]J. Britt and C. Ferekides, Appl. Phys. Lett. **62**, 2851 (1993).
[4]*Landolt-Bornstein: Numerical Data and Functional Relationships in Science and Technology*, edited by O. Madelung, M. Schulz, and H. Weiss (Springer, Berlin, 1982), Vol. 17b.
[5]J. Johansson, L. S. Karlsson, C. P. T. Svensson, T. Mårtensson, B. A. Wacaser, K. Deppert, L. Samuelson, and W. Seifert, Nature Mater. **5**, 574 (2006).
[6]A. Mikkelsen, N. Sköld, L. Ouattara, M. Borgström, J. N. Andersen, L. Samuelson, W. Seifert, and E. Lundgren, Nature Mater. **3**, 519 (2004).
[7]E. L. Wood and F. Sansoz, Nanoscale **4**, 5268 (2012).
[8]J. Bao, D. C. Bell, F. Capasso, J. B. Wagner, T. Mårtensson, J. Trägårdh, and L. Samuelson, Nano Lett. **8**, 836 (2008).
[9]Q. Li, X. Gong, C. Wang, J. Wang, K. Ip, and S. Hark, Adv. Mater. **16**, 1436 (2004).
[10]Y. Hao, G. Meng, Z. L. Wang, C. Ye, and L. Zhang, Nano Lett. **6**, 1650 (2006).
[11]B. Y. Geng, X. W. Liu, Q. B. Du, X. W. Wei, and L. D. Zhang, Appl. Phys. Lett. **88**, 163104 (2006).
[12]Q. Meng, C. Jiang, and S. X. Mao, J. Cryst. Growth **310**, 4481 (2008).
[13]X. Fan, X. M. Meng, X. H. Zhang, M. L. Zhang, J. S. Jie, W. J. Zhang, C. S. Lee, and S. T. Lee, J. Phys. Chem. C **113**, 834 (2009).
[14]B. L. Williams, D. P. Halliday, B. G. Mendis, and K. Durose, Nanotechnology **24**, 135703 (2013).
[15]Q. Xiong, J. Wang, and P. C. Eklund, Nano Lett. **6**, 2736 (2006).
[16]A. H. Carim, K. K. Lew, and J. M. Redwing, Adv. Mater. **13**, 1489 (2001).
[17]B. Liu, Y. Bando, C. Tang, F. Xu, J. Hu, and D. Golberg, J. Phys. Chem. B **109**, 17082 (2005).

[18]S.-M. Zhou, X. H. Zhang, X. M. Meng, X. Fan, K. Zou, and S.-K. Wu, Mater. Lett. **58**, 3578 (2004).
[19]C. Xu, J. Chun, K. Rho, H. J. Lee, Y. H. Jeong, D.-E. Kim, B. Chon, S. Hong, and T. Joo, Appl. Phys. Lett. **89**, 093117 (2006).
[20]C. X. Zhao, Y. F. Li, J. Zhou, L. Y. Li, S. Z. Deng, N. S. Xu, and J. Chen, Cryst. Growth Des. **13**, 2897 (2013).
[21]L. Jin, J. Wang, G. Cao, Z. Xu, S. Jia, W. C. H. Choy, Y. P. Leung, and T. I. Yuk, J. Phys. Chem. C **112**, 4903 (2008).
[22]J. Wang, M. Tian, T. E. Mallouk, and M. H. W. Chan, J. Phys. Chem. B **108**, 841 (2004).
[23]M. Murayama, Phys. Rev. B **49**, 4710 (1994).
[24]Y. Yan, M. M. Al-Jassim, K. M. Jones, S. H. Wei, and S. B. Zhang, Appl. Phys. Lett. **77**, 1461 (2000).
[25]S.-H. Wei, Phys. Rev. B **62**, 6944 (2000).
[26]A. De, Phys. Rev. B **81**, 155210 (2010).
[27]G. Jacopin, L. Rigutti, L. Largeau, F. Fortuna, F. Furtmayr, F. H. Julien, M. Eickhoff, and M. Tchernycheva, J. Appl. Phys. **110**, 064313 (2011).
[28]B. Ketterer, M. Heiss, E. Uccelli, J. Arbiol, and A. F. i Morral, ACS Nano **5**, 7585 (2011).
[29]J. Arbiol, S. Estradé, J. D. Prades, A. Cirera, F. Furtmayr, C. Stark, A. Laufer, M. Stutzmann, M. Eickhoff, M. H. Gass, A. L. Bleloch, F. Peiró, and J. R. Morante, Nanotechnology **20**, 145704 (2009).
[30]A. Plößl and G. Kräuter, Mater. Sci. Eng. R **25**, 1 (1999).
[31]M. Alexe and U. Gosele, *Wafer Bonding* (Springer, 2004).
[32]O. Moutanabbir and U. Gosele, Annu. Rev. Mater. Res. **40**, 469 (2010)
[33]S. H. Christiansen, R. Singh, and U. Gosele, Proc. IEEE **94**, 2060 (2006).
[34]A. Y. Belov, R. Scholz, and K. Scheerschmidt, Philos. Mag. Lett. **79**, 531 (1999).
[35]K. Scheerschmidt, D. Conrad, and A. Belov, Comput. Mater. Sci. **24**, 33 (2002).
[36]A. Y. Belov, K. Scheerschmidt, and U. Gosele, Phys. Status Solidi A **171**, 159 (1999).
[37]M. J. Kim and R. W. Carpenter, J. Electron. Mater. **32**, 849 (2003).
[38]M. J. Kim, R. W. Carpenter, M. J. Cox, and J. Xu, J. Mater. Res. **15**, 1008 (2000).
[39]U. Gosele, Y. Bluhm, G. Kastner, P. Kopperschmidt, G. Krauter, R. Scholz, A. Schumacher, S. Senz, Q. Y. Tong, L. J. Huang, Y. L. Chao, and T. H. Lee, J. Vac. Sci. Technol. A **17**, 1145 (1999).
[40]C. Chen, K. N. Tu, C. H. Tung, T. T. Sheng, A. Ploessl, R. Scholz, and U. Gosele, Philos. Mag. A **80**, 881 (2000).
[41]S. Heinemann, R. Wirth, M. Gottschalk, and G. Dresen, Phys. Chem. Miner. **32**, 229 (2005).
[42]K. Hartmann, R. Wirth, and W. Heinrich, Phys. Chem. Miner. **37**, 291 (2010).
[43]Y. S. Wu, C. R. Becker, A. Waag, R. Schmiedl, S. Einfeldt, and G. Landwehr, J. Appl. Phys. **73**, 7385 (1993).
[44]See supplementary material at http://dx.doi.org/10.1063/1.4844855 for identify the flats orientations by XRD, and HAADF images of the bonded interface.
[45]P. M. Kelly, C. J. Wauchope, and X. Zhang, Microsc. Res. Tech. **28**, 448 (1994).
[46]F. A. Kish, D. A. Vanderwater, M. J. Peanasky, M. J. Ludowise, S. G. Hummel, and S. J. Rosner, Appl. Phys. Lett. **67**, 2060 (1995).
[47]G. N. Yushin and Z. Sitar, Appl. Phys. Lett. **84**, 3993 (2004).
[48]G. E. Pike and C. H. Seager, J. Appl. Phys. **50**, 3414 (1979).